applied sciences

MDPI

Article

Two-Dimensional Modelling Approach for Electrokinetic Water Transport in Unsaturated Kaolinite

Rubén López-Vizcaíno *, Vicente Navarro and Ángel Yustres *

Geoenvironmental Group, Department of Civil Engineering and Construction, Civil Engineering School, University of Castilla-La Mancha, Avda. Camilo José Cela s/n, 13071 Ciudad Real, Spain
* Correspondence: ruben.lopezvizcaino@uclm.es (R.L.-V.); angel.yustres@uclm.es (Á.Y.)

Featured Application: This article presents a new version of the M4EKR code adapted for two-dimensional domains. The capabilities of the model were demonstrated in the analysis of operational parameters related to the location of electrodes and their geometrical distribution in application of electrokinetic techniques to unsaturated media.

Abstract: Although electrokinetic treatments for soil remediation and ground improvement have gradually undergone significant experimental development, one of the most important physical phenomena has received very little attention in recent years. Electroosmotic flow, especially in unsaturated conditions, has not been simulated in domains of more than one dimension. In the present work, a modification of the M4EKR code was used to study water movement in partially saturated soils under electrokinetic treatments. Two different configurations were studied: electrodes placed in electrolyte wells and electrodes directly inserted into the soil, and the treatment was started under unsaturated conditions for both. Due to the unrestricted availability of fluid in the first case, soil saturation is inevitable, but in the second case, only a spatial redistribution of water content can be observed. A detailed analysis of a variety of configurations involving several electrolyte wells showed that the number of electrodes, the distance between them and, above all, the ratio between the two magnitudes determines the efficiency of soil saturation and the energy consumed in the process.

Keywords: electrokinetic; electroosmosis; unsaturated soils; multiphysics simulation; M4EKR; two-dimensional; kaolinite

check for updates

Citation: López-Vizcaíno, R.; Navarro, V.; Yustres, Á. Two-Dimensional Modelling Approach for Electrokinetic Water Transport in Unsaturated Kaolinite. *Appl. Sci.* **2023**, *13*, 519. https://doi.org/10.3390/app13010519

Academic Editor: Angeles Sanroman Braga

Received: 11 November 2022
Revised: 5 December 2022
Accepted: 21 December 2022
Published: 30 December 2022

Copyright: © 2022 by the authors. Licensee MDPI, Basel, Switzerland. This article is an open access article distributed under the terms and conditions of the Creative Commons Attribution (CC BY) license (https://creativecommons.org/licenses/by/4.0/).

1. Introduction

In recent years, there has been a steady growth of cities, which has led to the use of land that was previously not intended for urban development. The most representative examples are (i) the occupation of rural land associated with agricultural and livestock activities located in flood plains or deltas [1], (ii) the use of former industrial land [2,3] and (iii) seaward expansion [4]. The first two cases are susceptible to finding contaminated land, either by agrochemicals or other compounds used in industrial production processes in the past. In addition, it is to be expected that highly deformable soils will be present (mainly in the first and third cases presented above), and consequently, significant ground settlement is to be expected.

For this reason, the research fields of soil remediation processes and ground improvement techniques are of current interest. In particular, the application of electrokinetic techniques may be an important option in the near future due to their well-known advantageous characteristics [5–7] and the fact that they can be installed at almost any location because they can be powered by renewable energy [8,9].

Numerical models for the simulation of electrokinetic treatments are very useful tools for the design, start-up, and operation of any technology. In addition, it is possible to

improve knowledge of the physical-electrochemical phenomena that take place (temperature increase due to the Joule effect, electromigration, electroosmosis, electrophoresis, electrolysis of water, electrooxidation of compounds, alteration of the geochemical equilibrium of the porewater, etc.) and predict the behaviour of the system under changes to or modifications of the operating conditions. However, due to the large number of phenomena occurring simultaneously, knowledge of the coupling of all these phenomena is still limited. For example, only in recent times has electroosmosis in porous media been deeply analysed from different perspectives, from nanofluidic approximation [10–14] to a more macroscopic approach [15–17]. Consequently, to reduce the complexity level involved in a total interaction, the models developed thus far have been designed to simulate isolated specific processes or with very limited couplings. As reported in several recently published reviews [18–20], electromigration and diffusive transport are covered in practically all conceptual models; however, electroosmotic transport is treated unevenly concerning the approach chosen, and many models even omit it. However, it has been identified that, in many works, the water mass balance is included or not included assuming saturated conditions. In any case, few models [21–29] explicitly study water transport due to the application of electric fields in partially saturated media. The group becomes even smaller for analyses conducted in a two-dimensional system. For this reason, there is an important demand in the soil electrokinetic treatment community for a tool to simulate water transport in soils under any condition of saturation.

In this context, this work presents an approach developed to reproduce the behaviour of partially saturated soils with low hydraulic permeability under the application of an external electric potential gradient. This approach was implemented on the platform COMSOL Multiphysics [30] as a new version of the M4EKR code [28,29] developed by the authors and adapted for the simulation of two-dimensional domains. The proposed conceptual model (coincident for one- and two-dimensional simulations) was previously validated for the simulation of water transport in partially saturated kaolin under electrical effects [31]. The numerical model presented in this work presents, for the first time, a 2D model for water mass transport, which allows for the evaluation of realistic soil treatment strategies. The model was used to investigate the influence of the disposition and location of the electrodes in the soil to be treated. Two alternatives are generally used in real practice: (i) direct insertion of the electrodes into the soil [32–34] or (ii) positioning of electrodes within electrolyte reservoirs [35–39]. Regardless of the option selected, the electrodes can be distributed in the soil using many different configurations, such as rows, alternating fences, or other geometrical distributions [27,40–44]. Taking these aspects into account, in the present work, a sensitivity analysis of the hydraulic behaviour of the system was carried out according to the initial degree of saturation of the soil and the applied electric potential gradient, as well as an analysis of the final energy consumption. The capabilities of the model allow for the analysis of the spatial distribution of water in the soil and the magnitude of the fluxes and analysis of the different phenomena involved. In this way, the model makes it possible to identify the relevant parameters for the arrangement of the electrodes in an electrokinetic soil treatment.

2. Materials and Methods

2.1. Mathematical Model

2.1.1. Water Transport

The temporal and spatial distribution of the mass of water contained in a partially saturated soil was obtained by solving a standard mass conservation equation, as shown below:

$$\frac{\partial m_w}{\partial t} + \nabla \cdot \mathbf{l}_w = 0 \quad (1)$$

where m_w is the mass of water per unit of total volume, $\mathbf{l}_w$ is the mass flux of water, and $\nabla \cdot$ is the divergence operator.

The mass of water per unit of total volume is defined as:

$$m_{\mathrm{w}} = \phi Sr \rho_{\mathrm{w}} \tag{2}$$

where ϕ is the porosity of the soil, Sr is the degree of soil saturation, and ρ_{w} is the water density. In a general form, the mass flux of water in this system, $\mathbf{l}_{\mathrm{w}}$, is the sum of the hydraulic flux, $\mathbf{l}_{\mathrm{w}}^{\mathrm{h}}$, and the electroosmotic flux, $\mathbf{l}_{\mathrm{w}}^{\mathrm{eo}}$, defined by the following expressions:

$$\mathbf{l}_{\mathrm{w}} = \mathbf{l}_{\mathrm{w}}^{\mathrm{h}} + \mathbf{l}_{\mathrm{w}}^{\mathrm{eo}} \tag{3}$$

$$\mathbf{l}_{\mathrm{w}}^{\mathrm{h}} = \rho_{\mathrm{w}} \mathbf{q}_{\mathrm{w}}^{\mathrm{h}} \tag{4}$$

$$\mathbf{l}_{\mathrm{w}}^{\mathrm{eo}} = \rho_{\mathrm{w}} \mathbf{q}_{\mathrm{w}}^{\mathrm{eo}} \tag{5}$$

where $\mathbf{q}_{\mathrm{w}}^{\mathrm{h}}$ and $\mathbf{q}_{\mathrm{w}}^{\mathrm{eo}}$ are the hydraulic and electroosmotic volumetric fluxes, respectively. The hydraulic volumetric flux is defined using Darcy's law (without including the effect of gravity since the two-dimensional domain is a horizontal plane), which considers the liquid pressure gradient as the driving force for the transport of water by this phenomenon:

$$\mathbf{q}_{\mathrm{w}}^{\mathrm{h}} = -\frac{K^{\mathrm{h}}}{\rho_{\mathrm{w}} g} \nabla P_{\mathrm{L}} \tag{6}$$

where ∇ is the gradient differential operator, g is the gravitational constant, P_{L} is the liquid pore pressure, and K^{h} is the effective hydraulic permeability of the porous media. The electroosmotic volumetric flux is calculated as:

$$\mathbf{q}_{\mathrm{w}}^{\mathrm{eo}} = -K^{\mathrm{eo}} \nabla \psi \tag{7}$$

where ψ is the electric potential and K^{eo} is the effective electroosmotic permeability of the porous media. Both effective permeabilities are calculated as the product of a saturated conductivity ($K_{\mathrm{sat}}^{\mathrm{h}}$ for the hydraulic conductivity and $K_{\mathrm{sat}}^{\mathrm{eo}}$ for the electroosmotic conductivity) and a relative permeability function, k_{rel}, expressed as a Brooks and Corey [45] type power function with an exponent of 3. In this case, the driving force for water transport by electroosmosis is the electric potential gradient.

To simulate the temporal evolution of the volume from electrolyte reservoirs, additional water balance equations in these compartments were formulated using the following expression:

$$\frac{\partial V_{\mathrm{R}}}{\partial t} = \overline{\mathrm{q}}_{\mathrm{R}} H_{\mathrm{R}} \tag{8}$$

where H_{R} is the height of the electrolyte reservoir and $\overline{\mathrm{q}}_{\mathrm{R}}$ is calculated by means of the closed line integral:

$$\overline{\mathrm{q}}_{\mathrm{R}} = \oint \mathbf{q}_{\mathrm{w}} \cdot \mathbf{n} \, ds \tag{9}$$

where $\mathbf{n}$ is the outwards vector normal to the reservoir boundary (reservoir wall) and $\mathbf{q}_{\mathrm{w}}$ can be defined as:

$$\mathbf{q}_{\mathrm{w}} = \mathbf{q}_{\mathrm{w}}^{\mathrm{h}} + \mathbf{q}_{\mathrm{w}}^{\mathrm{eo}} \tag{10}$$

2.1.2. Electric Charge Transport

Assuming that the application of an external electric potential gradient does not produce any phenomenon that generates a charge accumulation in the soil [46] and that the system initially starts from an electrically balanced condition, the electric charge balance can be expressed as:

$$\nabla \cdot \mathbf{i} = 0 \tag{11}$$

where $\mathbf{i}$ is the current density, which is calculated as:

$$\mathbf{i} = -\sigma_{\mathrm{a}} \nabla \psi \tag{12}$$

where σ_a is the apparent electrical conductivity of the partially saturated soil. The influence of the porosity and degree of saturation has been considered by estimating the apparent electrical conductivity by an expression based on Archie's second law [47,48]:

$$\sigma_a = \frac{1}{a_A \phi^{-m_A} Sr^{-B}} \tag{13}$$

where a_A and m_A are Archie's constants that depend on the nature of the soil and B is the saturation index [48].

The energy consumption in the electrokinetic treatment, E, is calculated according to the following time integral:

$$E = \int I \Delta\psi_{el} H_R dt \tag{14}$$

where $\Delta\psi_{el}$ is the electric potential difference between electrodes and I corresponds to the integrated value:

$$\mathrm{I} = \oint \mathbf{i} \cdot \mathbf{n}\, ds \tag{15}$$

which is analogous to the closed line integral of Equation (9) for the calculation $\overline{q}_R$.

2.2. Numerical Model Implementation

The proposed conceptual model corresponds to a new version of the M4EKR tool, which is fully implemented in COMSOL Multiphysics [30]. As in other previous adaptations of the M4EKR code, all equations were implemented using the constitutive models presented in Section 2.1; therefore, no preprogrammed COMSOL modules were used. In the simulations, two partial differential equations for the mass balance of water in the soil and the electric charge balance were solved. P_L and ψ were selected as state variables. In addition, N + 1 ordinary differential equations (ODEs) were used to solve the variation in the electrolyte volume in the 'N' reservoirs present in each simulation and an additional ODE for calculation of the energy consumption.

The above equations are solved simultaneously using a monolithic, fully coupled approach. COMSOL Multiphysics controls the preprocessing (discretization, initial, and boundary conditions), operates the solver of the system of the set of partial and ordinary differential equations, and manages the postprocessing of the results.

2.3. Description of the Modelled Materials

Kaolinite was selected as a representative material of low hydraulic permeability soil in the simulations carried out in this work. This clay mineral has been extensively characterised in the literature. For instance, in a previous work [31], the authors determined a set of empirical expressions to calculate the saturated hydraulic and electroosmotic conductivities as functions of the soil void ratio:

$$K_{sat}^{h}\left(\mathrm{m\ s^{-1}}\right) = 3.329{\cdot}10^{-9} e - 2.151{\cdot}10^{-9} \tag{16}$$

$$K_{sat}^{eo}\left(\mathrm{m^2\ s^{-1}\ V^{-1}}\right) = 6.101{\cdot}10^{-9} e - 3.615{\cdot}10^{-9} \tag{17}$$

The dependence of the degree of saturation on the matric suction (s) is modelled using the van Genuchten approach [49]:

$$Sr = \left(1 + (\alpha s)^n\right)^{-m} \tag{18}$$

where the matric suction is defined as the difference between the gas pressure, P_G, and the liquid pressure, P_L. When P_L is close to P_G, the suction nears zero, and consequently (taking into account the Van Genuchten approach), Sr tends to 1. Therefore, this model is valid for simulating fully saturated soils.

In summary, Table 1 presents the parameters used in the present work for the modelling of kaolinite.

Table 1. Characterisation parameters for the modelled kaolinite.

Parameter	Description	Unit	Value
α *	Van Genuchten parameter	kPa^{-1}	2.39×10^{-3}
n *	Van Genuchten parameter	-	1.8423
m *	Van Genuchten parameter	-	0.4572
a_A **	Archie parameter	Ωm	2.356
m_A **	Archie parameter	-	5.639
B **	Saturation index	-	2.744
ρ_s	Density of mineral particles	$kg\ m^{-3}$	2650
w_{ini}	Initial water content	-	0.25

* From [31]; ** From [47].

2.4. Description of the Simulation Exercises

An extensive series of simulation exercises were carried out to analyse the capabilities of the presented numerical tool. All simulations were performed using a two-dimensional domain (50 cm wide by 70 cm long), a mid-plane of the mock-up installation used in previous works [35,36,39,50]. Figure 1 shows a scheme of all the electrode configurations simulated in this work.

First, the electrohydraulic behaviour was analysed as a function of the distribution of the electrodes in the soil to be treated. For this purpose, simulations were carried out using a simple electrode configuration with a single anode facing a cathode under two different approaches: both inside electrolyte reservoirs (Figure 1a) or both directly inserted into the soil (Figure 1b). In the former approach, it was assumed that the electrolyte has a high electrical conductivity, and therefore, potential losses between the electrode and the soil can be neglected. Table 2 shows the initial and boundary conditions for the simulation approach.

Table 2. Initial and boundary conditions.

		Electrodes into the Soil		Electrodes into the Electrolyte Reservoirs	
		Anode	**Cathode**	**Anolyte Reservoir**	**Catholyte Reservoir**
Initial cond.	Electrical (V)	$\psi = 0$ V		$\psi = 0$ V	
	Hydraulic (kPa)	$P_L = P_{L,\,ini}$		$P_L = P_{L,\,ini}$	
Boundary cond.	Electrical (V)	$\psi = \psi_{anode}$	$\psi = 0$ V	$\psi = \psi_{anode}$	$\psi = 0$ V
	Hydraulic (kPa)	No flux		$P_L = P_{atm} = 100$ kPa	
Electrode/reservoir radius		0.005 m		0.02 m	
Electrode/reservoir height		0.1 m			

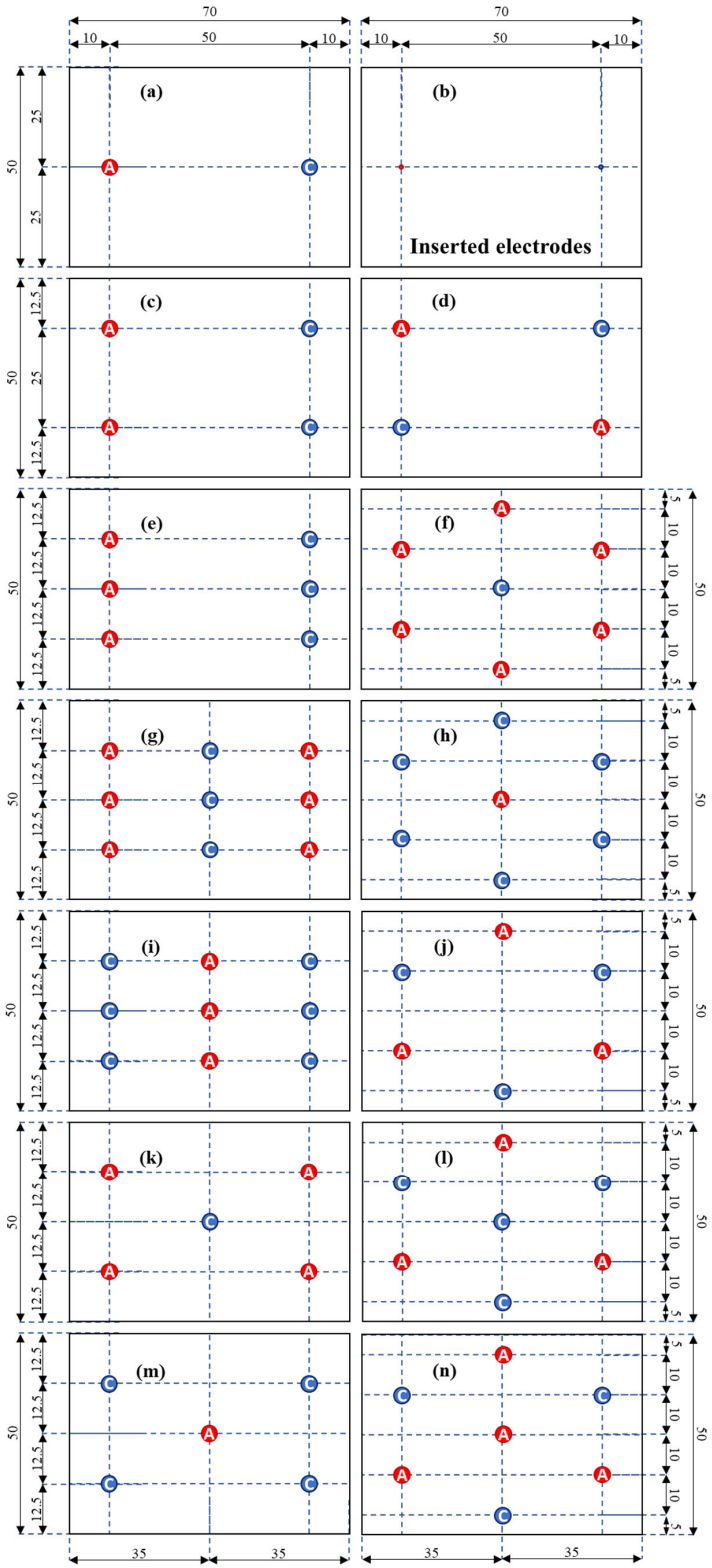


Figure 1. Schemes of the simulated electrode configurations. (**a**) opposed electrodes in electrolyte reservoirs; (**b**) opposed electrodes inserted into the soil; (**c**–**n**) alternative distributions of electrodes inserted in electrolyte reservoirs. A in red is for anode(s) and C in blue is for cathode(s).

The hydraulic initial condition is given by the initial value of the state variable of the water mass balance equation: the liquid pressure. The initial water content, the void ratio,

and the density of solid particles are known, and therefore, with this information, the initial degree of saturation can be calculated as:

$$Sr_{\text{ini}} = \frac{w_{\text{ini}}\rho_{\text{s}}}{e\rho_{\text{w}}} \tag{19}$$

Based on the definition of Sr, it is also possible to obtain the initial matric suction by rearranging the van Genuchten expression of the water retention curve, Equation (18), as

$$s_{\text{ini}} = \frac{\left(Sr_{\text{ini}}^{-1/m} - 1\right)^{1/n}}{\alpha} \tag{20}$$

Assuming that P_{G} is constant, and equal to atmospheric pressure (P_{atm}), the initial liquid pressure, $P_{\text{L, ini}}$ can be calculated by the expression:

$$P_{\text{L, ini}} = P_{\text{atm}} - s_{\text{ini}} \tag{21}$$

The initial electric potential gradient is zero in all simulations as the soil is initially electrically balanced.

The boundary conditions depend on the configuration of the system: electrodes located in electrolyte reservoirs and electrodes inserted in the soil. These conditions are applied either on the electrolyte reservoir or the electrode surface, respectively. The electric boundary conditions are intended to simulate the application of an external potential gradient between two points. For this purpose, Dirichlet-type boundary conditions that set the electric potential at the cathode/catholyte reservoir to zero have been imposed, while the electric potential applied in the anode/anolyte reservoir (ψ_{anode}) is calculated as the product of the electric potential gradient and the minimum distance between pairs of anodes/cathodes. Non-flux boundary conditions are set for all the external walls of the simulated domain.

For hydraulic boundary conditions, a non-flux condition (Neumann type) was applied in the simulations where the electrodes are inserted into the soil, as no addition/extraction of water occurs in this configuration, and to the external walls. However, when using electrolytic wells, the usual practice is to maintain constant electrolyte levels in the reservoirs, which are usually open to the atmosphere. This can be simulated by applying a Dirichlet boundary condition such as $P_{\text{L}} = P_{\text{atm}} = 100$ kPa (see Table 2).

In both configurations, a sensitivity analysis of both the void ratio (simulating three cases with different void ratio values [47]: 0.7, 0.9 and 1.2) and the applied electric potential gradient (simulating three potential gradients: 1, 10 and 50 Vcm^{-1}) was carried out. Table S1 presents the values of the physical parameters as a function of the void ratio range studied.

Second, the influence of the geometrical arrangement of the electrodes when they are placed inside electrolyte reservoirs was assessed. For this purpose, 12 additional cases were simulated with different configurations, both in terms of the number of electrodes and their spatial distribution (Figure 1). These cases were analysed with two different electric potential gradients, 1 and 50 Vcm^{-1}, in a soil with a void ratio of 0.9. The initial and boundary conditions used are specified in Table 2. The parameters used to compare the performance between these electrode configurations were the energy consumption required to reach a state of total saturation of the soil and the time necessary to reach this state.

3. Results and Discussion

3.1. Influence of the Electrode Positioning Type

3.1.1. Void Ratio Sensitivity

Three simulations were carried out by setting the void ratio at 0.7, 0.9, and 1.2. As the initial water content was the same in the three cases (0.25, see Table 1), the initial degree of saturation for each simulation was 0.946, 0.736, and 0.552, respectively. The electric potential gradient applied was 1 Vcm^{-1} in the three cases.

First, progressive saturation of the soil was observed in the simulations when electrolyte reservoirs were considered. To explain this behaviour, it is important to bear in mind that, in general, a constant electrolyte level is maintained in the reservoir during the process. In the experimental setups, this is achieved with level controllers coupled with solenoid valves that allow for the addition/extraction of electrolyte. Considering this, and starting from a partially saturated state, a liquid pressure gradient was induced from the electrolyte reservoirs to the soil in contact with them, producing a significant hydraulic flow that generates soil saturation. This behaviour has been observed in previous experimental tests focused on electrokinetic remediation of pesticide-contaminated soils. Two-dimensional moisture distribution maps show a progressive and homogeneous increase in this variable [50,51]. Different time intervals are needed to reach full saturation depending on the initial degree of saturation. For a time of 86,400 s (1 d), the case with e = 0.7 presented an average saturation degree of 0.963, while for the cases with e = 0.9 and e = 1.2, the values were 0.841 and 0.721, respectively.

By inspecting Figure 2, it is apparent that water transport by electroosmosis is not relevant, since no asymmetries in the isolines of the degree of saturation can be observed. When an analysis of the net volume change of electrolytes was carried out (Figure 3), a loss of volume from both the anolyte and catholyte to the soil was observed in the first stages. The trend was more pronounced in the case where saturation was lower. However, while this volume loss was maintained in the case of anolyte reservoirs, a turning point appeared in the variation of the volume of the catholyte. From that moment onwards, an increase in the volume of catholyte was associated with a net transport of water from the soil to this reservoir. This indicates a change in the predominant type of water transport phenomenon, switching from hydraulic to electroosmotic. To explain this behaviour, it is useful to analyse the evolution of the volumetric fluxes (Figure 4).

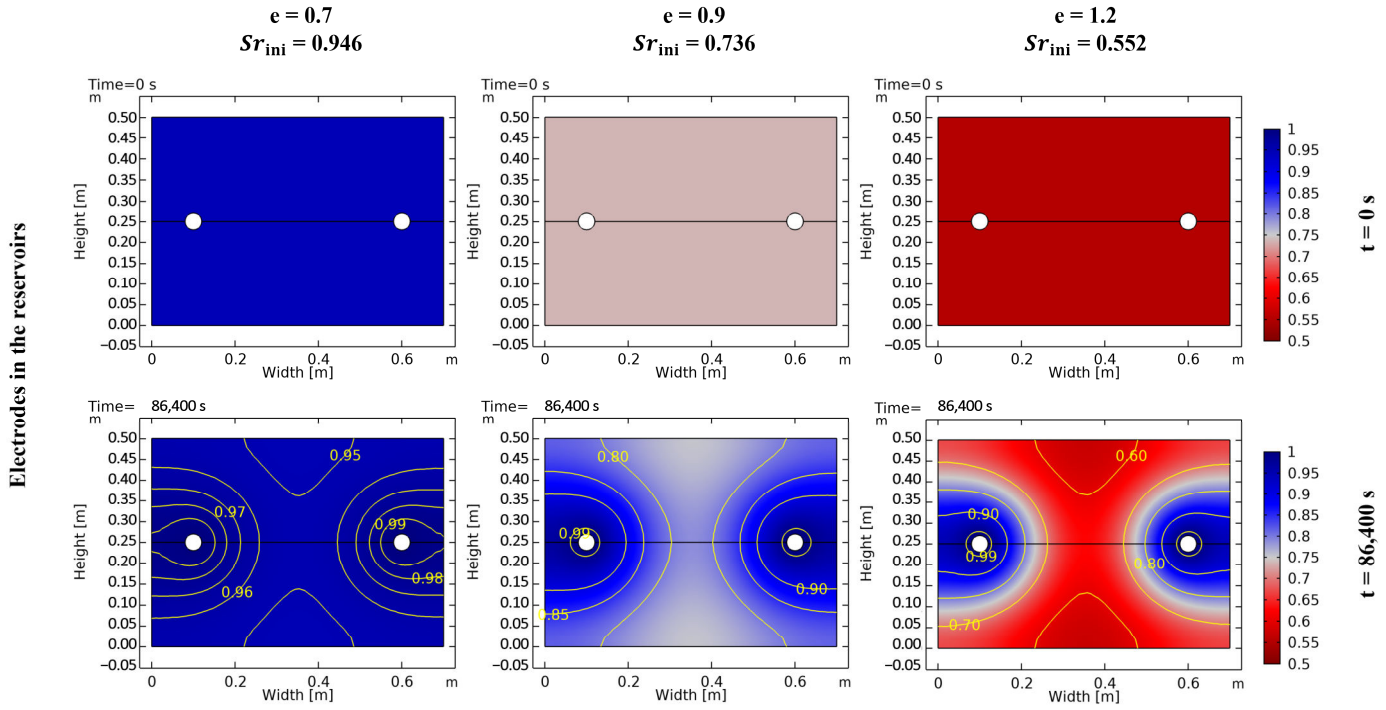


Figure 2. 2D maps of the degree of saturation evaluated at two times, 0 and 86,400 s (1 d), and three void ratios, 0.7, 0.9, and 1.2, when the electrodes were placed into the electrolyte reservoirs corresponding to the configuration presented in Figure 1a. Electric potential gradient: 1 Vcm^{-1}.

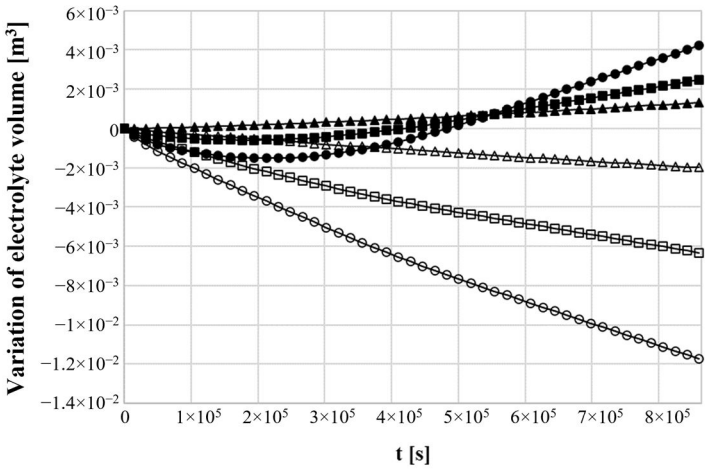


Figure 3. Temporal variation of anolyte (empty markers) and catholyte (filled marker) volume. Void ratio: 0.7 ▲, 0.9 ■, 1.2 ●.

In the cases of void ratios of 0.9 and 1.2, at t = 86,400 s (1 d), it can be observed that the hydraulic volumetric flow was much higher than the electroosmotic flow. However, at t = 864,000 s (10 d), the time at which full saturation was reached in all three simulated cases, the liquid pressure remained constant and equal to atmospheric pressure in both the soil and the electrolyte reservoirs. Consequently, there is no liquid pressure gradient, and therefore, the Darcian transport is negligible compared to the electroosmotic flow, whose direction is from anode to cathode, as shown in Figure 4. In addition, the direct influence of the degree of saturation on the magnitude of electroosmotic flow can be verified. The electroosmotic transport was higher when the soil was saturated (t = 864,000 s) than when it was in a state of partial saturation (t = 86,400 s). On the other hand, increases in both the electroosmotic and hydraulic volumetric fluxes associated with an increase in the void ratio were also observable, fundamentally due to the dependence of the saturated conductivities on the void ratio.

Finally, it is important to highlight the significant increase observed in the magnitude of both fluxes in the vicinity of the electrolyte reservoirs. In the case of the hydraulic flux, this occurs because the highest liquid pressure gradient is present in this zone. However, in the case of the electroosmotic flow, it is mainly due to a simple geometrical effect associated with the two-dimensional configuration. The area of origin/arrival of the electric current lines (the circular orifice corresponds to the electrolyte reservoirs) is smaller than the total area of the domain through which they flow. Consequently, a flow concentration is produced around these areas, thus increasing the current density and consequently the electric potential gradient.

The second scenario corresponds to electrodes inserted directly into the soil. In this case, no addition or withdrawal of electrolyte from the system was carried out. Figure 5 shows the evolution of the degree of saturation for the three different void ratios.

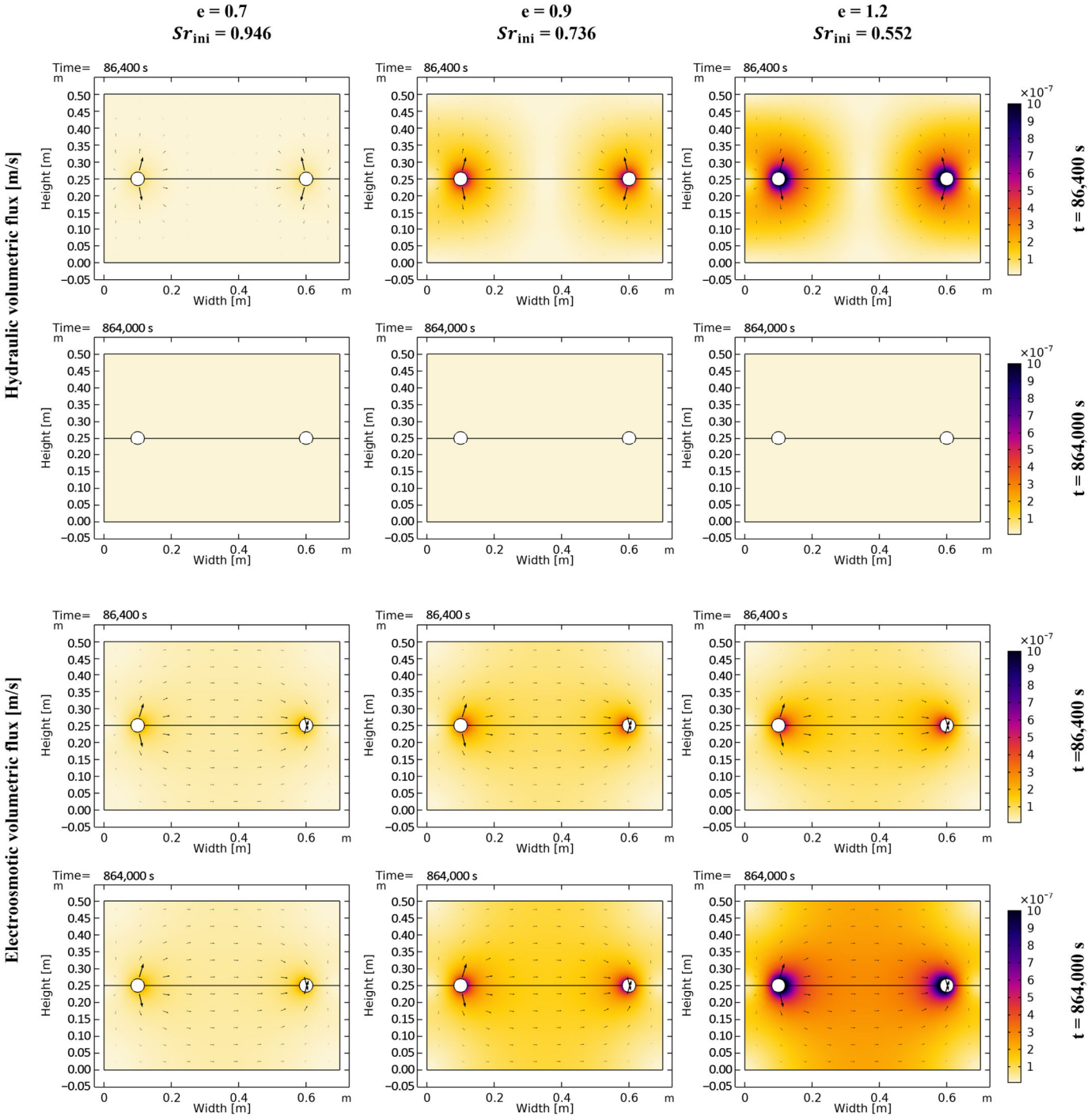


Figure 4. 2D maps of hydraulic and electroosmotic volumetric fluxes evaluated at two times, 86,400 (1 d) and 864,000 s (10 d), and three void ratios, 0.7, 0.9, and 1.2, when the electrodes were in the electrolyte reservoirs, as shown in Figure 1a. Electric potential gradient applied: 1 Vcm^{-1}.

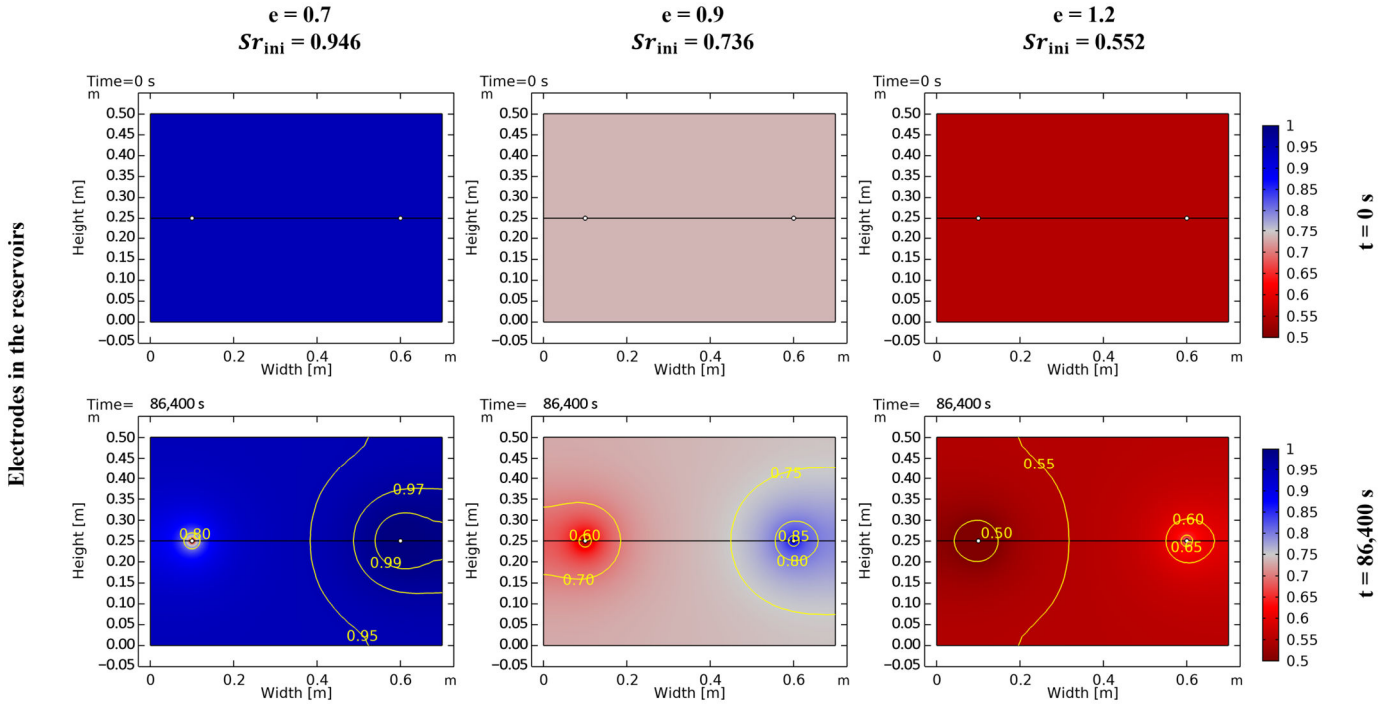


Figure 5. 2D maps of the degree of saturation evaluated at two times, 0 and 86,400 s (1 d), and three void ratios, 0.7, 0.9, and 1.2, when the electrodes were inserted into the soil corresponding to the configuration presented in Figure 1b. An electric potential gradient of 1 Vcm^{-1} was applied.

The behaviour observed in this scenario was totally different from that obtained when electrolyte reservoirs are used. In this case, there was a redistribution of the water content of the system. There was progressive drying of the area near the anode and, on the other hand, an increase in the degree of saturation in the area where the cathode was located. This phenomenon has also been shown in experimental tests evaluating the electrokinetic removal of phenolic compounds in partially saturated soils. The normalised evolution of the water content shows a desiccation near the anode and an increase at the cathode side [33,34]. This behaviour can be explained by taking into account the direction of water transport by electroosmosis, which is the predominant transport phenomenon when using this technique (see Supplementary Material Figure S2).

3.1.2. Electric Potential Gradient Sensitivity

For the sensitivity analysis, three additional simulations were carried out by fixing the void ratio at 0.9 and applying electric potential gradients of 5, 10, and 50 Vcm^{-1}. The initial water content of the soil was the same in the three cases (0.25, see Table 1); therefore, the initial degree of saturation for each simulation was 0.736. Figure 6 shows the saturation degree for the three simulated cases.

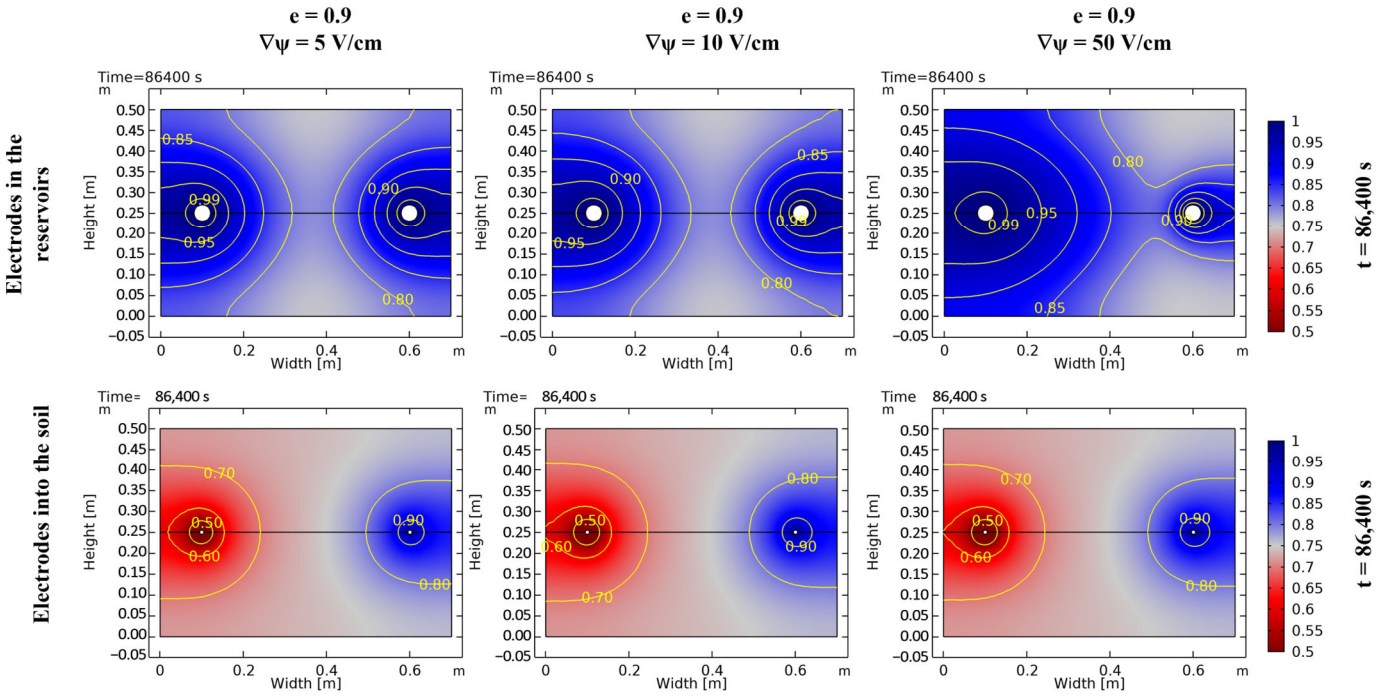


Figure 6. 2D maps of the degree of saturation evaluated at 86,400 s and three electric potential gradients of 5, 10, and 50 Vcm^{-1}: 0.7, 0.9, and 1.2 when the electrodes were in the electrolyte reservoirs and inserted into the soil corresponding to the configurations presented in Figure 1a and 1b, respectively. The void ratio of soil was 0.9.

In the electrolyte reservoir scenario, it can be observed that as the applied electric potential gradient increased, the process of saturation of the soil discussed above was accelerated from the anolyte reservoir zone. This shows that the contribution of the electroosmosis process to the net water transport is more significant. In the corresponding scenario with direct insertion of the electrodes, the effect is not as relevant. Although a higher electric potential gradient generates a higher electroosmotic flux, in this case, the redistribution of the water content within the soil produces liquid pressure gradients and consequently gives rise to fluxes opposite to the electroosmotic ones. Therefore, the effect of an increase in the electric potential gradient is counterbalanced in this type of system.

3.2. Influence of the Applied Electrode Configuration

In a previous study, it was found that under the operating conditions set when using electrolyte reservoirs, kaolinite tends to saturate. At that point, the electroosmotic flow becomes the most relevant contribution to the total flow. Two magnitudes were selected as reference indicators to elucidate the influence of the electrode arrangement on the saturation process: (i) the amount of energy required to reach a fully saturated state and (ii) the time required to do so. Twelve configurations were selected (together with the basic distribution used in the previous sections of this work, Figure 1a,c–n), which are the most common configurations found in the literature [27,40–44]. Simulations were carried out by applying electric potential gradients of 1 and 50 Vcm^{-1}. To establish a common criterion that facilitates comparison, the electric potential applied in the anolyte reservoir (ψ_{anode}) was estimated by considering the minimum distance between anode/cathode pairs. Table 3 presents the main features of the simulations conducted in this study.

Table 3. Characteristics of the simulations for electrode configuration analysis.

Configuration	Anode/Cathode	Total Electrodes	Minimum Distance [m]	ψ_{anode} [V] $\nabla\psi$=1 Vcm^{-1}	ψ_{anode} [V] $\nabla\psi$=50 Vcm^{-1}	Electrode/ Distance
Figure 1a	1/1	2	0.5	50	2500	4
Figure 1c	2/2	4	0.5	50	2500	8
Figure 1d	2/2	4	0.2	20	1000	20
Figure 1e	3/3	6	0.5	50	2500	12
Figure 1f	6/1	7	0.2	20	1000	35
Figure 1g	6/3	9	0.25	25	1250	36
Figure 1h	1/6	7	0.2	20	1000	35
Figure 1i	3/6	9	0.25	25	1250	36
Figure 1j	3/3	6	0.2	20	1000	30
Figure 1k	4/1	5	0.2795	27.95	1397.5	17.89
Figure 1l	3/4	7	0.2	20	1000	35
Figure 1m	1/4	5	0.2795	27.95	1397.5	17.89
Figure 1n	4/3	7	0.2	20	1000	35

There is a decreasing trend in the time required to achieve full saturation of the soil as the total number of electrolyte reservoirs increases (Figure 7a). Furthermore, even when the electrical gradient was applied and the number of electrodes were the same, there were cases with very different saturation times. For example, in a system with 6 electrodes, specifically 3 anodes and 3 cathodes, the configuration corresponding to Figure 1e (2 rows of 3 electrodes facing each other) presented a saturation time almost double that obtained in the configuration illustrated in Figure 1j (hexagonal geometry with alternating anodes and cathodes). This reveals that, in addition to the number of electrolyte reservoirs, the geometrical configuration also has a significant influence. If the saturation time is analysed as a function of the minimum distance between anodes and cathodes, small interelectrode distances result in shorter saturation times. Even so, in this case, the trend is not clear, as there was greater dispersion among the results obtained. This dispersion decreases if the saturation time is analysed as a function of the electrode/minimum distance ratio, where a well-defined decreasing trend in saturation time was observed as the ratio increases. Of all the electrode configurations used, one (corresponding to the diagram in Figure 1d) displayed a behaviour discordant with the general trend. This may indicate that the number of electrodes has a more important role than the minimum distance between anode–cathode pairs in the time needed to reach saturation.

Regarding the energy consumption in the saturation process, the trends observed coincide with those corresponding to the time needed. It is important to highlight the energy increase observed (up to three orders of magnitude) when a potential gradient of 50 Vcm^{-1} was applied. However, the reduction in the time needed to saturate the soil was not as relevant compared to the simulations carried out at 1 Vcm^{-1}.

From the above results, it could be stated that for the simulated cases, the type of electrode configuration used has a greater relevance in the transport of water through a partially saturated soil than the applied electric potential gradient.

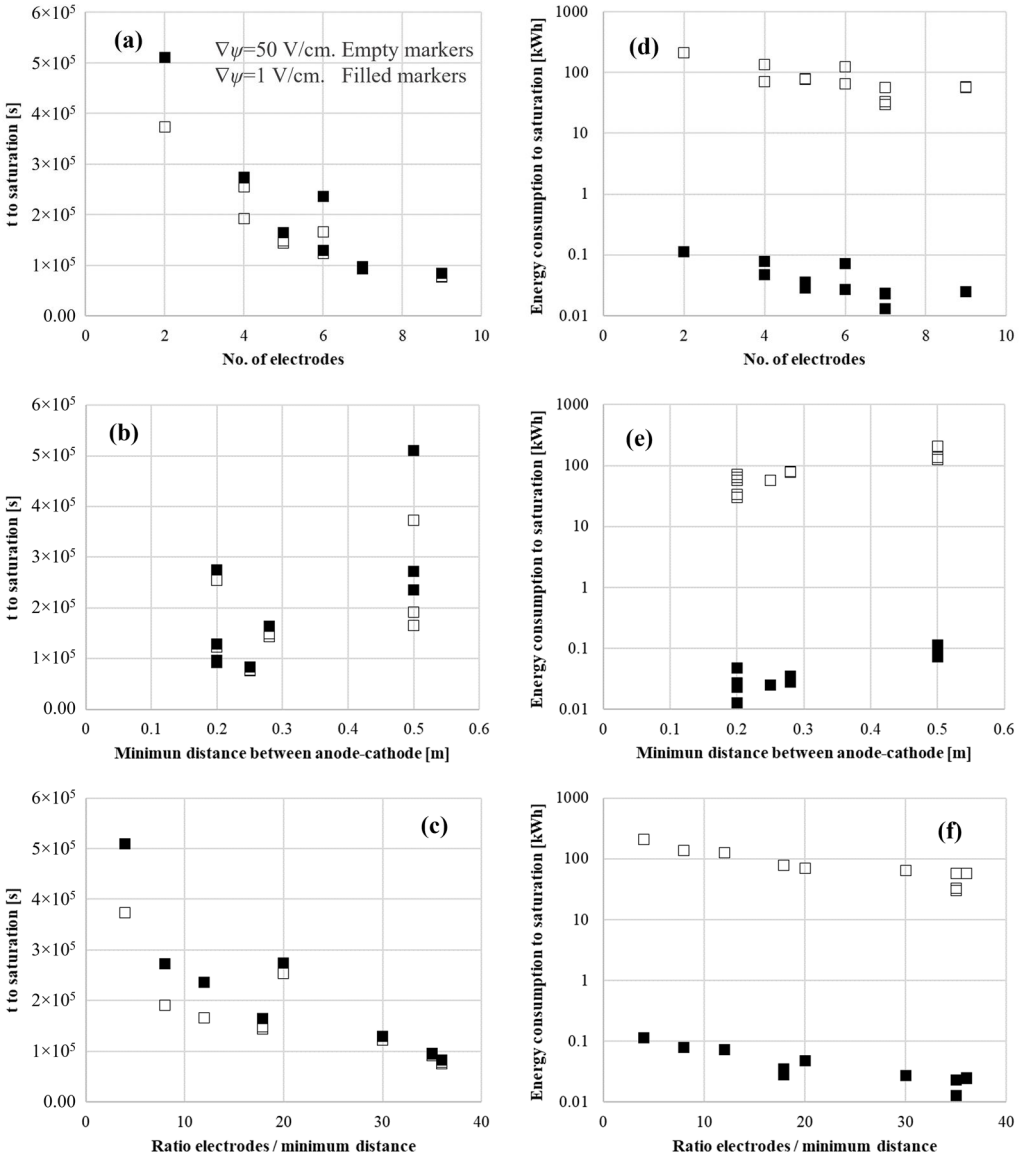


Figure 7. Time to saturation depending on the (**a**) number of total electrodes, (**b**) minimum distance between the anode–cathode, and (**c**) ratio of electrodes/minimum distance. Energy consumption to saturation depending on the (**d**) number of total electrodes, (**e**) minimum distance between the anode–cathode, and (**f**) ratio of electrodes/minimum distance. $\nabla\psi = 50$ Vcm^{-1} is indicated by empty markers and $\nabla\psi = 1$ Vcm^{-1} is indicated by filled markers.

4. Conclusions

In this paper, a new conceptual model and a simulation tool were developed that allow for the simulation of water flow in partially saturated soils in 2D domains under electrokinetic treatments. With a simple formulation and state functions based on the extensive characterisation that has been developed over time for kaolinite, different operational alternatives were analysed. This has allowed for the identification of behavioural trends and the optimisation of treatment strategies on a lab scale. Relevant differences in performance were observed between operation with electrolyte wells, which provide unlimited fluid supply, and operation with electrodes inserted in the ground. In the first case, saturation of the soil is almost inevitable, and a higher fluid flow in the soil is reached after this point. This configuration is particularly suitable for electroosmotic flushing of contaminants or for the delivery of reactants in ground improvement techniques in low-permeability soils. In the second case, there is only a redistribution of water within the soil, so this arrangement

is ideal for soil dewatering and drainage, which can be advantageous in improving the mechanical properties of the ground.

In addition, a detailed analysis of various operating alternatives with several electrolyte wells and varying spatial distributions was carried out. It was found that the ratio of the number of electrodes to the minimum distance between them primarily determines both the time to saturation and the energy consumption. It has been shown that electrical potential gradients do not particularly favour rapid saturation of the soil, and greatly increase the energy cost. This implies that there is an important task of optimisation in the design of these kinds of treatments. Optimal designs are also expected to be dependent on the properties of the soil to be treated, its volume, the available energy sources, and the type of treatment to be conducted. The role of numerical models is therefore fundamental in the process of fine-tuning and optimising electrokinetic treatments, although practical experience in the field will always be irreplaceable.

However, the presented numerical model still suffers from limitations. In particular, more tests are needed for its validation. In general, most of the tests thus far have focused on evaluation of the reduction in pollutant concentration (electrokinetic remediation) or the variation in the soil void ratio (electroconsolidation). In future works, it will be essential to have reliable results on the spatial distribution of water content in situations with well-defined initial and boundary conditions. Furthermore, an additional extension to 3D conditions and more realistic geometries will be required to fully exploit the capabilities of this model.

Supplementary Materials: The following supporting information can be downloaded at: https://www.mdpi.com/article/10.3390/app13010519/s1, Figure S1: 2D maps of the current density and electric potential gradient for the configuration presented in Figure 1a. Figure S2: 2D maps of hydraulic and electroosmotic volumetric fluxes for the configuration presented in Figure 1b. Table S1: Values of the physical parameters as a function of the void ratio range studied.

Author Contributions: Conceptualization: R.L.-V. and Á.Y.; methodology: R.L.-V. and Á.Y.; software: R.L.-V. and Á.Y.; formal analysis and investigation: R.L.-V., Á.Y. and V.N.; writing—original draft preparation: R.L.-V.; writing—review and editing: R.L.-V., Á.Y. and V.N.; funding acquisition: Á.Y., V.N. and R.L.-V., supervision: V.N. and Á.Y.; project administration: Á.Y. and V.N. All authors have read and agreed to the published version of the manuscript.

Funding: This research was funded by: (i) MCIN/AEI/10.13039/501100011033- Spanish National Research Agency, grant number [PID2020–118291RB-I00] and (ii) University of Castilla-La Mancha and European Social Fund plus (ESF+), grant number [2022-POST-20890].

Institutional Review Board Statement: Not applicable.

Informed Consent Statement: Not applicable.

Data Availability Statement: Data available on request from the authors.

Acknowledgments: We thank Maria Mavroulidou for the kind invitation to participate in this Special Issue.

Conflicts of Interest: The authors declare no conflict of interest.

References

1. Radwan, T.M.; Blackburn, G.; Whyatt, J.; Atkinson, P.M. Global land cover trajectories and transitions. *Sci. Rep.* **2021**, *11*, 12814. [CrossRef] [PubMed]
2. Chiang, S.Y.D.; Gu, Q. Brownfield sites remediation technology overview, trends, and opportunities in China. *Remediat. J.* **2015**, *25*, 85–99. [CrossRef]
3. Coulon, F.; Jones, K.; Li, H.; Hu, Q.; Gao, J.; Li, F.; Chen, M.; Zhu, Y.; Liu, R.; Liu, M.; et al. China's soil and groundwater management challenges: Lessons from the UK's experience and opportunities for China. *Environ. Int.* **2016**, *91*, 196–200. [CrossRef]
4. Dhritiraj, S.; Chen, R.; Meadows, M.E. Building beyond land: An overview of coastal land reclamation in 16 global megacities. *Appl. Geogr.* **2018**, *90*, 229–238.

5. Reddy, K.R.; Cameselle, C. *Electrochemical Remediation Technologies for Polluted Soils, Sediments and Groundwater*; John Wiley and Sons: Hoboken, NJ, USA, 2009.
6. Rodrigo, M.A.; Santos, E.V.D. (Eds.) *Electrochemically Assisted Remediation of Contaminated Soils. Fundamentals, Technologies, Combined Processes and Pre-Pilot and Scale-up Applications*; Environmental Pollution; Springer Nature Switzerland AG: Cham, Switzerland, 2021.
7. Ribeiro, A.B.; Prasad, M. (Eds.) *Electrokinetic Remediation for Environmental Security and Sustainability*; Wiley: Hoboken, NJ, USA, 2021.
8. Fernandez-Marchante, C.M.; Souza, F.; Millan, M.; Lobato, J.; Rodrigo, M.A. Can the green energies improve the sustainability of electrochemically-assisted soil remediation processes? *Sci. Total Environ.* **2021**, *803*, 149991. [CrossRef] [PubMed]
9. Millan, M.; Bucio-Rodriguez, P.; Lobato, J.; Fernandez-Marchante, C.; Roa-Morales, G.; Barrera-Diaz, C.; Rodrigo, M.A. Strategies for powering electrokinetic soil remediation: A way to optimize performance of the environmental technology. *J. Environ. Manag.* **2020**, *267*, 110665. [CrossRef] [PubMed]
10. Mondal, P.K.; Roy, M. Spreadsheet analysis of the field-driven start-up flow in a microfluidic channel. *Electrophoresis* **2021**, *42*, 2465–2473. [CrossRef]
11. Mondal, P.K.; Ghosh, U.; Bandopadhyay, A.; Dasgupta, D.; Chakraborty, S. Electric-field-driven contact-line dynamics of two immiscible fluids over chemically patterned surfaces in narrow confinements. *Phys. Rev. E—Stat. Nonlinear Soft Matter Phys.* **2013**, *88*, 023022. [CrossRef]
12. Mondal, P.K.; DasGupta, D.; Bandopadhyay, A.; Ghosh, U.; Chakraborty, S. Contact line dynamics of electroosmotic flows of incompressible binary fluid system with density and viscosity contrasts. *Phys. Fluids* **2015**, *27*, 032109. [CrossRef]
13. Gogoi, A.; Reddy, K.; Mondal, P.K. Electro-osmotic flow through nanochannel with different surface charge configurations: A molecular dynamics simulation study. *Phys. Fluids* **2021**, *33*, 092115. [CrossRef]
14. Gaikwad, H.S.; Baghel, P.; Sarma, R.; Mondal, P.K. Transport of neutral solutes in a viscoelastic solvent through a porous microchannel. *Phys. Fluids* **2019**, *31*, 022006. [CrossRef]
15. Gan, Q.; Zhou, J.; Tao, Y.; Jiang, Y. Interfacial resistance model for electro-osmotic system. *Geotechnique* **2022**. [CrossRef]
16. Zhou, J.; Gan, Q.; Tao, Y. Electro-osmotic permeability model based on ions migration. *Acta Geotech.* **2022**, *17*, 2379–2393. [CrossRef]
17. Yustres, Á.; López-Vizcaíno, R.; Cabrera, V.; Rodrigo, M.; Navarro, V. Donnan-ion hydration model to estimate the electroosmotic permeability of clays. *Electrochim. Acta* **2020**, *355*, 136758. [CrossRef]
18. Isidro, J.; López-Vizcaíno, R.; Yustres, A.; Sáez, C.; Navarro, V.; Rodrigo, M.A. Recent progress in physical and mathematical modelling of electrochemically assisted soil remediation processes. *Curr. Opin. Electrochem.* **2022**, *36*, 101115. [CrossRef]
19. López-Vizcaíno, R.; Yustres, Á.; Cabrera, V.; Navarro, V. Conceptual and mathematical modeling of the transport of pollutants in soil by electric fields. In *Electrochemically Assisted Remediation of Contaminated Soils: Fundamentals, Technologies, Combined Processes and Pre-Pilot and Scale-Up Applications*; Rodrigo, M.A., Santos, E.V.D., Eds.; Springer International Publishing: Cham, Switzerland, 2021; pp. 59–85.
20. Maria, V.-G.; del Mar Cerrillo-Gonzalez, M.; Paz-Garcia, J.M.; Rodriguez-Maroto, J.M. An overview of the modeling of electrokinetic remediation. In *Electrokinetic Remediation for Environmental Security and Sustainability*; Ribeiro, A.B., Prasad, M.N.V., Eds.; Wiley: Hoboken, NJ, USA, 2021; pp. 1–34.
21. Milad, R.; Asadollahfardi, G.; Gomez-Lahoz, C.; Villen-Guzman, M.; Paz-Garcia, J.M. Modeling of electrokinetic remediation of Cd- and Pb-contaminated kaolinite. *J. Hazard. Mater.* **2019**, *366*, 630–635.
22. Cristina, J.; Cattaneo, F.; Musso, G.; Tamagnini, C.; Salciarini, D. Multiphysics modeling of electrokinetic phenomena in unsaturated fine–grained soils. In *Multiscale and Multiphysics Processes in Geomechanics*; Springer: Berlin/Heidelberg, Germany, 2011; pp. 89–92.
23. Paz-García, J.M.; Johannesson, B.; Ottosen, L.; Alshawabkeh, A.; Ribeiro, A.; Rodríguez-Maroto, J.M. Modeling of electrokinetic desalination of bricks. *Electrochim. Acta* **2012**, *86*, 213–222. [CrossRef]
24. Paz-García, J.M.; Johannesson, B.; Ottosen, L.; Ribeiro, A.; Rodríguez-Maroto, J.M. Simulation-based analysis of the differences in the removal rate of chlorides, nitrates and sulfates by electrokinetic desalination treatments. *Electrochim. Acta* **2013**, *89*, 436–444. [CrossRef]
25. Gry, S.; Ottosen, L.M.; Jensen, P.E.; Paz-Garcia, J.M. Electrochemical desalination of bricks—Experimental and modeling. *Electrochim. Acta* **2015**, *181*, 24–30.
26. Tao, M.; Pan, T. A Multiphysics model for evaluating electrokinetic remediation of nuclear waste-contaminated soils. *Water Air Soil Pollut.* **2015**, *226*, 77.
27. Benitez, A.G.; Bento, N.J.S.; Neves, T.A.; Santos, F.S.; Silva, G.C.; de Sousa, P.A.P. Numerical study of the influence of electrode arrangements in electrokinetic remediation technique. *Environ. Sci. Pollut. Res.* **2017**, *24*, 26424–26435.
28. López-Vizcaíno, R.; Yustres, A.; León, M.; Saez, C.; Cañizares, P.; Rodrigo, M.; Navarro, V. Multiphysics implementation of electrokinetic remediation models for natural soils and porewaters. *Electrochim. Acta* **2017**, *225*, 93–104. [CrossRef]
29. Ángel, Y.; López-Vizcaíno, R.; Cabrera, V.; Navarro, V. M4ekr, multiphysics for electrokinetic remediation of polluted soils. In Proceedings of the 4th European Conference on Unsaturated Soils (E-UNSAT 2020), Lisbon, Portugal, 24–26 June 2020.
30. COMSOL AB. *Comsol Multiphysics Reference Manual Version: Comsol 5.1*; COMSOL AB: Stockholm, Sweden, 2015.

31. Yustres, Á.; López-Vizcaíno, R.; Sáez, C.; Cañizares, P.; Rodrigo, M.; Navarro, V. Water transport in electrokinetic remediation of unsaturated kaolinite. Experimental and numerical study. *Sep. Purif. Technol.* **2018**, *192*, 196–204. [CrossRef]
32. Jones Colin, J.F.P.; Lamont-Black, J.; Glendinning, S. Electrokinetic geosynthetics in hydraulic applications. *Geotext. Geomembr.* **2011**, *29*, 381–390. [CrossRef]
33. Luo, Q.; Zhang, X.; Wang, H.; Qian, Y. Mobilization of phenol and dichlorophenol in unsaturated soils by non-uniform electrokinetics. *Chemosphere* **2005**, *59*, 1289–1298. [CrossRef] [PubMed]
34. Luo, Q.; Zhang, X.; Wang, H.; Qian, Y. The use of non-uniform electrokinetics to enhance in situ bioremediation of phenol-contaminated soil. *J. Hazard. Mater.* **2005**, *121*, 187–194. [CrossRef] [PubMed]
35. López-Vizcaíno, R.; Alonso, J.; Cañizares, P.; León, M.; Navarro, V.; Rodrigo, M.; Sáez, C. Removal of phenanthrene from synthetic kaolin soils by eletrokinetic soil flushing. *Sep. Purif. Technol.* **2014**, *132*, 33–40. [CrossRef]
36. López-Vizcaíno, R.; Alonso, J.; Cañizares, P.; León, M.J.; Navarro, V.; Rodrigo, M.A.; Sáez, C. Electroremediation of a natural soil polluted with phenanthrene in a pilot plant. *J. Hazard. Mater.* **2014**, *265*, 142–150. [CrossRef]
37. Risco, C.; López-Vizcaíno, R.; Sáez, C.; Yustres, A.; Cañizares, P.; Navarro, V.; Rodrigo, M.A. Remediation of soils polluted with 2,4-D by electrokinetic soil flushing with facing rows of electrodes: A case study in a pilot plant. *Chem. Eng. J.* **2016**, *285*, 128–136. [CrossRef]
38. Risco, C.; Rodrigo, S.; López-Vizcaíno, R.; Sáez, C.; Cañizares, P.; Navarro, V.; Rodrigo, M.A. Electrokinetic flushing with surrounding electrode arrangements for the remediation of soils that are polluted with 2,4-D: A case study in a pilot plant. *Sci. Total Environ.* **2016**, *545–546*, 256–265. [CrossRef]
39. Risco, C.; Rubí-Juárez, H.; Rodrigo, S.; Vizcaíno, R.L.; Saez, C.; Cañizares, P.; Barrera-Díaz, C.; Navarro, V.; Rodrigo, M.A. Removal of oxyfluorfen from spiked soils using electrokinetic fences. *Sep. Purif. Technol.* **2016**, *167*, 55–62. [CrossRef]
40. Vocciante, M.; Caretta, A.; Bua, L.; Bagatin, R.; Ferro, S. Enhancements in electrokinetic remediation technology: Environmental assessment in comparison with other configurations and consolidated solutions. *Chem. Eng. J.* **2016**, *289*, 123–134. [CrossRef]
41. Xu, H.; Cang, L.; Song, Y.; Yang, J. Influence of electrode configuration on electrokinetic-enhanced persulfate oxidation remediation of pah-contaminated soil. *Environ. Sci. Pollut. Res.* **2020**, *27*, 44355–44367. [CrossRef]
42. Kim, W.S.; Park, G.; Kim, D.; Jung, H.; Ko, S.; Baek, K. In situ field scale electrokinetic remediation of multi-metals contaminated paddy soil: Influence of electrode configuration. *Electrochim. Acta* **2012**, *86*, 89–95. [CrossRef]
43. Alshawabkeh, A.N.; Gale, R.; Ozsu-Acar, E.; Bricka, R.M. Optimization of 2-D electrode configuration for electrokinetic remediation. *J. Soil Contam.* **1999**, *8*, 617–635. [CrossRef]
44. Kim, S.O.; Jeong, J.; Lee, W.; Yun, S.; Jo, H.Y. Electrokinetic remediation of heavy metal-contaminated soils: Performance comparison between one- and two-dimensional electrode configurations. *J. Soils Sediments* **2021**, *21*, 2755–2769. [CrossRef]
45. Brooks, R.H.; Corey, A. *Hydraulic Properties of Porous Media*; Colorado State University: Fort Collins, CO, USA, 1964.
46. Jacobs, R.A.; Probstein, R.F. Two-dimensional modeling of electroremediation. *AIChE J.* **1996**, *42*, 1685–1696. [CrossRef]
47. Rafaela, C.; Dias, A.S. Study of the electrical resistivity of compacted kaolin based on water potential. *Eng. Geol.* **2017**, *226*, 1–11.
48. Ahmed, K.M.; Santos, F.A.M. Influence of degree of saturation in the electric resistivity–hydraulic conductivity relationship. *Surv. Geophys.* **2009**, *30*, 601.
49. van Genuchten, M.T. Closed-form equation for predicting the hydraulic conductivity of unsaturated soils. *Soil Sci. Soc. Am. J.* **1980**, *44*, 892–898. [CrossRef]
50. Risco, C.; Rubí-Juárez, H.; Rodrigo, S.; López-Vizcaíno, R.; Saez, C.; Cañizares, P.; Barrera-Díaz, C.; Navarro, V.; Rodrigo, M.A. Removal of oxyfluorfen from spiked soils using electrokinetic soil flushing with the surrounding arrangements of electrodes. *Sci. Total Environ.* **2016**, *559*, 94–102. [CrossRef] [PubMed]
51. Risco, C.; Rodrigo, S.; López-Vizcaíno, R.; Yustres, A.; Sáez, C.; Cañizares, P.; Navarro, V.; Rodrigo, M.A. Electrochemically assisted fences for the electroremediation of soils polluted with 2,4-D: A case study in a pilot plant. *Sep. Purif. Technol.* **2015**, *156*, 234–241. [CrossRef]

Disclaimer/Publisher's Note: The statements, opinions and data contained in all publications are solely those of the individual author(s) and contributor(s) and not of MDPI and/or the editor(s). MDPI and/or the editor(s) disclaim responsibility for any injury to people or property resulting from any ideas, methods, instructions or products referred to in the content.